THE ASTROPHYSICAL JOURNAL, 344:146–157, 1989 September 1

SOLVING THE VLASOV EQUATION IN GENERAL RELATIVITY

FREDERIC A. RASIO,[1] STUART L. SHAPIRO,[1,2] AND SAUL A. TEUKOLSKY[1,2]
Center for Radiophysics and Space Research, Cornell University
Received 1988 September 29; accepted 1989 February 7

ABSTRACT

We have developed a new numerical method for determining the dynamical evolution of a collisionless system in full general relativity. The method exploits Liouville's theorem to determine the evolution of the distribution function of matter in phase space directly. The distribution function is governed by the collisionless Boltzmann (Vlasov) equation coupled to Einstein's equations for the gravitational field. The method accurately tracks the increasingly complicated, fine-grained structure developed by the distribution function due to phase mixing. It can be used to study Newtonian as well as fully relativistic systems. We restrict our analysis to spherically symmetric systems in this paper, but the gravitational field can be arbitrarily strong and the matter velocities arbitrarily close to the speed of light. Applications include violent relaxation, the stability of relativistic star clusters, and the collapse of unstable relativistic star clusters to black holes.

Subject headings: galaxies: nuclei — gravitation — relativity — stars: stellar dynamics

I. INTRODUCTION

Recently, Shapiro and Teukolsky (1985*a*, *b*, *c*, 1986; hereafter ST1, ST2, ST3, ST4, respectively) have demonstrated how to calculate numerically (at least in spherical symmetry) the dynamical evolution of self-gravitating, collisionless systems in general relativity. Their method yields a solution to the collisionless Boltzmann (Vlasov) equation coupled to Einstein's equations for the gravitational field.

Collisionless relativistic systems may very well exist in nature. Quasars, active galactic nuclei (AGNs), and other intense extragalactic radio sources are believed to be powered by supermassive black holes (see, e.g., Begelman, Blandford, and Rees 1984). But the formation of these supermassive black holes remains a mystery. This is a topical issue, since there is now solid observational evidence (see Dressler and Richstone 1988; Kormendy 1988) that the nuclei of some nearby galaxies do indeed contain massive ($M \gtrsim 10^6\ M_\odot$) black holes. It has long been recognized (see Zel'dovich and Podurets 1965) that such massive black holes can form as a consequence of the dynamical instability of a relativistic star cluster. In ST3 (see also Kochanek, Shapiro, and Teukolsky 1987; Quinlan and Shapiro 1988), recent Newtonian Fokker-Planck calculations of the gravothermal catastrophe, together with the relativistic calculations of ST1 and ST2, were recombined to make such a scenario more than plausible. Cosmology also provides us with several possible candidates for astrophysical realizations of relativistic collisionless systems. Dark galactic halos made of weakly interactive massive particles (WIMPs) are but one example.

In their previous papers, ST addressed several major unresolved issues concerning collisionless gases in general relativity. Among these were the stability criterion for spherical relativistic star clusters and the nonlinear evolution and final fate of unstable clusters, including gravitational collapse to black holes and relativistic violent relaxation. It had been conjectured that the onset of instability for spherical relativistic star clusters coincides with the first maximum of the fractional binding energy along an appropriately constructed one-parameter sequence (see Fackerell 1970; Ipser and Thorne 1968; Ipser 1969*a*, *b*, 1980). This was indeed confirmed by the numerical calculations (see ST2). Moreover, it was found that most unstable clusters undergo gravitational collapse to black holes on a dynamical time scale. The physical properties of these resulting black holes could even be studied in detail (see ST4). These results suggest that collisionless systems will provide a wealth of new possibilities for numerical relativity and constitute an essential complement to other studies focusing mainly on fluid systems (see, e.g., Smarr 1979, or Centrella 1985 for discussion and references) and scalar fields (see Choptuik 1986).

The computational method of ST combined the techniques of numerical relativity with those of N-body particle simulations. In their method, a statistical representation of the initial distribution function is constructed by specifying initial positions and velocities for a large but finite number N of discrete particles. The motion of these particles is then calculated by integrating simultaneously N geodesic equations in the mean gravitational field of the system. The source terms of the Einstein equations, written in the ADM formalism, are determined by smearing out each particle over a small spatial volume, and adding up the contributions of all particles. This is basically a relativistic generalization of the particle-mesh methods (also called "particle-in-cell methods" in the context of plasma physics) used to study Newtonian collisionless star clusters (see Sellwood 1987 for an excellent review).

Particle methods have the characteristic feature that all numerical calculations are done in *real space*, even though they are used to solve the collisionless Boltzmann equation, which expresses the evolution of a system in phase *space*. It is in fact impossible, with particle methods, to determine the distribution function f of a system in phase space, since these methods only produce *moments* of f. The information provided by particle methods is therefore very incomplete. The full knowledge of f is required to define the dynamical state of a system uniquely. Many complicated phenomena of great astrophysical interest, such as violent relaxation or the collisionless damping of per-

[1] Department of Physics, Cornell University.
[2] Department of Astronomy, Cornell University.

turbations by phase mixing, can only be understood by a detailed study of the *phase space evolution* of a system.

It is usually assumed in particle methods that the particles "naturally" provide an adequate statistical coverage of phase space. However, it is not clear to what extent a particle simulation (especially with small N) actually reproduces the solution of the collisionless Boltzmann equation, which in some sense should correspond to the $N \to \infty$ limit. For any finite value of N, artificial random statistical fluctuations will be present in all computed quantities. Recently there has been some indication that these fluctuations can sometimes lead to spurious results. For example, Nishida (1986) found that the bar instability of a thin stellar disk can be suppressed by the presence of a small bulge component, even though previous particle simulations had led to the opposite conclusion (see also Sellwood 1986; White 1988).

Another possibility to study collisionless systems is to use what we will refer to as a "phase space method" (Sellwood 1987 uses the term "collisionless Boltzmann code" instead). A phase space method does not rely on any statistical representation of the system by particles. Instead, *a phase space method explicitly constructs the (smooth) distribution function of matter in phase space.* The source terms of the field equations are directly obtained by numerical quadratures of f over velocity space. This has the great advantage of eliminating random statistical fluctuations in the data while at the same time providing us with the full distribution function of the system. Unfortunately, very few phase space methods have so far been successfully developed, even in the much simpler framework of Newtonian gravity, and all of them are still in their infancy. The reason is the extreme complexity of working in phase space instead of real space. The large number of dimensions in phase space (already three in spherical symmetry where real space has only one) would already discourage many attempts. In addition, distribution functions often have rather irregular structures that can be hard to accurately represent numerically (e.g., on a grid in phase space). Such irregular structures can be due to the presence of discontinuities in the initial data, but even in the case of a very smooth initial data, phase mixing will usually produce increasingly intricate "fine-grained" structures (see, e.g., Fig. 5 below).

Given these difficulties, it is not surprising that no one has attempted to develop a phase space method in the framework of general relativity, where further important complications are introduced by the need to integrate forward in time Einstein's equations for the gravitational field. This paper demonstrates how one can construct such a method and apply it to solve various problems in astrophysics and general relativity. For the first time we present the evolution of the distribution function of matter in phase space for several fully relativistic self-gravitating systems. These first results are restricted to spherical symmetry, but the matter velocity can approach the speed of light and the gravitational field can become arbitrarily strong. In particular, several cases include catastrophic collapse of the system to a black hole.

In § II, we summarize previous approaches for developing phase space methods and introduce a new scheme that proved essential in our own (relativistic) calculations. In § III, we write the basic equations of the problem and specialize them to spherical symmetry. This is done using the ADM formalism of general relativity. Section IV gives a detailed description of our numerical code. In § V we present several applications involving both Newtonian and relativistic calculations.

II. PHASE SPACE METHODS

a) Previous Approaches

We now briefly review previous attempts at developing phase space methods. We will confine ourselves here to the *gravitational* literature. However, most of the methods described here were originally invented by plasma physicists in a somewhat different context. It should be noted that today phase space methods have been essentially abandoned by plasma physicists, who systematically prefer particle simulations (see review by Dawson 1983).

Following Lynden-Bell's (1967) statistical theory of violent relaxation, which predicted the most probable final state of a collisionless self-gravitating system, a large effort was mounted to develop numerical techniques to calculate the dynamical evolution of such systems and verify directly Lynden-Bell's predictions (see Cuperman and Harten 1972; and references therein). Since this requires following phase space densities in detail, including all distortions due to phase mixing, phase space methods were needed. The first to be developed were the so-called "water bag" methods (Hohl and Feix 1967; Cupermann, Harten, and Lecar 1971). These methods can only be used to study one-dimensional systems. They are based on the following picture: matter in the two-dimensional (x, v_x) phase space is subdivided into a small (typically just one or two) number of domains. The distribution function $f(x, v_x, t)$, viewed as the density of an incompressible "phase fluid" is assumed to be constant within each domain (hence the name "water bag"). By Liouville's theorem, this density is conserved in time, so that one only has to follow the motion of the domain's boundaries in order to determine the evolution of the system. This is done numerically by taking a sufficiently large number of points on the boundary curves and moving them as test particles in the gravitational field of the system. With time, each boundary curve stretches and the system spreads out in phase space. Consequently, more and more points must be added in order to maintain a given accuracy. Since the computer-time consumption is a linearly increasing function of the number of points to be moved, it can increase more than linearly with physical time. This is not a defect of the method, but simply reflects the actual rapid increase of complexity taking place in the system. Water bag methods are the ideal tool for studying collisionless systems up to the point where they develop very large degrees of phase mixing. In spite of their severe limitations, they are still in use today for this purpose (see Luwel and Severne 1985).

A totally different approach consists in solving only the *lowest moments* of the collisionless Boltzmann equation. Recently this approach was followed by White and Woodward (1983), who reported some preliminary one-dimensional calculations (White 1986). In their method, phase phase is divided into a Eulerian (fixed) grid. In each zone of the grid, the distribution function is represented as a quadratic polynomial in the phase space coordinates, the coefficients of which are determined by all the possible moments of the distribution function up to second order. The moments are updated by calculating their fluxes across zone boundaries, so that mass, momentum, and energy are conserved exactly. This represents the major advantage of this method. However, when the structure of the distribution function in phase space is too fine for the grid to resolve, this method does not give a correct solution to the collisionless Boltzmann equation, since it imposes an artificial coarse graining.

A more straightforward approach to the problem is to resort to finite difference techniques, constructing again the distribution function on an Eulerian grid in phase space plus time. This is obviously limited to very low dimensions, and satisfactory finite difference schemes for the collisionless Boltzmann equation have actually been developed only in two-dimensional phase spaces. In more than two phase space dimensions, an attempt was made by Shlosman, Hoffman, and Shaviv (1979; see also Hoffman *et al.* 1979) in the context of spherically symmetric (Newtonian) star clusters. They used an explicit, two-step Lax-Wendroff scheme to solve the collisionless Boltzmann equation in a three-dimensional phase space. (By using the conserved angular momentum as one of the coordinates, the problem can actually be reduced to solving the collisionless Boltzmann equation in a two-dimensional phase space, as noted by Fujiwara 1983.) As expected, such a straightforward approach in higher dimensions met important difficulties. Conservation of mass and total energy were hard to reproduce numerically, because these are nonlocal quantities and cannot be conserved locally by the difference scheme. Even the positivity of the distribution function could not be guaranteed without resorting to a rather unnatural (at least unphysical) numerical filtering technique.

We believe that none of the methods described above can be generalized in a satisfactory way to study relativistic problems, where most of the computational effort should be spent in solving Einstein's equations and not in determining the distribution of matter. Especially, the necessity of using a Eulerian mesh in phase space appears to us as a most undesirable feature.

b) *Using Liouville's Theorem*

For both Newtonian and relativistic systems, the collisionless Boltzmann equation can always be written in the generic form:

$$\frac{\partial f(x, v, t)}{\partial t} + u[f]\,\frac{\partial f(x, v, t)}{\partial x} + a[f]\,\frac{\partial f(x, v, t)}{\partial v} = 0\,, \quad (1)$$

where the "velocity" $u[f]$ and "acceleration" $a[f]$ are known functionals of the distribution function f. The four basic steps to propagate the distribution function f from time t_1 to $t_2 > t_1$ are typically: (1) compute the source terms for the field equations (e.g., the density) by integrating f at t_1 over velocity space; (2) integrate the field equations, thereby determining $u[f]$ and $a[f]$ at time t_1; (3) extrapolate to determine (guess) the value of these quantities over the interval (t_1, t_2); finally (4) compute f at time t_2 using equation (1). A key idea in what follows will be to use Liouville's theorem for step (4), which we write as

$$f(x_2, v_2, t_2) = f(x_1, v_1, t_1)\,, \quad (2)$$

where (x_1, v_1) is the position in phase space at time t_1 of a test particle that *will reach* the position (x_2, v_2) at time t_2. Since $u[f]$ and $a[f]$ are known for all $t \leq t_2$, one can actually *construct* the trajectory of such a test particle. Since f is also known at all times $t \leq t_2$ one can therefore determine $f(x_2, v_2, t_2)$ for all (x_2, v_2).

This idea was first implemented in a numerical scheme developed by Fujiwara (1981, 1983). The elegance and simplicity of his method motivated us to develop its relativistic generalization. However, we quickly discovered that in many cases this scheme presents numerical instabilities which can lead to totally inaccurate results. We now describe why this happens, and how a more reliable scheme based on the ideas developed above can still be obtained.

In Fujiwara's method, the distribution function f is constructed on a *grid of points* in phase space. To get the value of f at time t_2 and grid point position (x_2, v_2), equation (2) is used with $t_1 = t_2 - \Delta t$, where Δt is the time step. The old position (x_1, v_1) is determined by placing a test particle at (x_2, v_2) and moving it backward in time, from t_2 to t_1, in phase space. In general, this old position (x_1, v_1) is not a grid point at time t_1. Therefore one must perform a (multidimensional) *interpolation* on the grid in order to get $f(x_1, v_1, t_1)$ and thereby the new grid point value $f(x_2, v_2, t_2)$. The error due to the interpolation on the grid at t_1 propagates to the new grid at t_2 where it becomes an error on the values of f *at the grid points*. This leads inevitably to an amplification of the error. In particular, mass or total energy are not conserved, and the positivity of the distribution function can be violated. When the distribution function presents discontinuities, or when it has developed even only a mild degree of phase mixing, the error due to just one interpolation can become quite large and the method breaks down almost immediately. This can be quite spectacular, especially if one uses spline interpolation, which tends to form large-amplitude oscillations whenever the data to be interpolated present any kind of strongly nonpolynomial behavior. (These severe problems were also recognized by Inagaki, Nishida, and Sellwood 1984; Nashida 1986; and White 1986.)

One very simple way of not having to use any interpolation is to extend the value of t_1 in equation (2) to $t = 0$. Indeed, at $t = 0$ to the distribution function f is known *to arbitrary accuracy*, since it must be given as an initial condition. Moreover, there is no need in this case to introduce *any grid at all* in phase space, since intermediate values of f are never needed and therefore need not be stored. One can directly compute all quadratures over velocity space at any time by using a *self-adaptive* quadrature routine. When the routine asks for the value of f at some point in phase space, this point is simply tracked along a dynamical path all the way back to $t = 0$, where f can be accurately evaluated from the initial data. Moreover, such a self-adaptive quadrature routine is *ideally suited* to problems involving discontinuous distribution functions or large degrees of phase mixing: more points can be added in phase space to maintain high accuracy whenever and wherever required by the structure of the distribution function. The only disadvantage of this scheme is its obviously large computational cost. Indeed, the computation time *per iteration* increases with time, since longer and longer trajectories have to be constructed to evaluate f at a given point. However, we have already argued that, at least to some extent, this merely reflects the real increase of complexity occurring in the physical system.

In § IV, we will give a detailed description of how these ideas have been implemented in our relativistic code. In particular, we will discuss a series of refinements that can be used to keep the total computation time within reasonable limits.

III. MATHEMATICAL FORMULATION

We adopt the notations of Misner, Thorne, and Wheeler (1973; hereafter MTW) and set $c = G = 1$ throughout.

a) *Basic Equations*

In general relativity, we define the distribution function as follows (see, e.g., Ipser and Thorne 1968). Consider a small element of matter near a particular event x in spacetime, and

with four-momentum near a particular value $\boldsymbol{p}$. As seen in its own rest frame, this matter element occupies a three-dimensional volume dV_x in spatial coordinate space and a four-dimensional volume dV_p in momentum space. If there are dN particles (or stars) in this matter element, then the number density in phase space, or distribution function $f(\boldsymbol{x}, \boldsymbol{p})$, is defined by

$$f(\boldsymbol{x}, \boldsymbol{p}) = \frac{dN}{dV_x\, dV_p} . \tag{3}$$

In coordinate form dV_x and dV_p are given by

$$dV_x = \frac{p^0}{m}\sqrt{-g}\, dx^1\, dx^2\, dx^3 ,$$

$$dV_p = \frac{-dp_0\, dp_1\, dp_2\, dp_3}{\sqrt{-g}} , \tag{4}$$

where g is the determinant of the metric and $m = (-p_\alpha p^\alpha)^{1/2}$ is the rest mass of a particle with four-momentum $\boldsymbol{p}$. For collisionless matter, particles move along geodesics, and Liouville's theorem implies the conservation of f along geodesics. This may be written (following MTW)

$$\frac{Df}{d\tau} = 0 , \tag{5}$$

where the Liouville operator $D/d\tau$ is differentiation with respect to proper time along a geodesic:

$$\frac{D}{d\tau} \equiv \left(\frac{dx^\alpha}{d\tau}\right)\frac{\partial}{\partial x^\alpha} + \left(\frac{dp_\alpha}{d\tau}\right)\frac{\partial}{\partial p_\alpha} = \frac{g^{\alpha\mu}p_\mu}{m}\frac{\partial}{\partial x^\alpha} - \frac{1}{2m}\, g^{\mu\nu}{}_{,\alpha}\, p_\mu p_\nu \frac{\partial}{\partial p_\alpha} . \tag{6}$$

Equation (5) represents the relativistic generalization of the collisionless Boltzmann equation. The metric $g_{\mu\nu}$ is determined by Einstein's equations,

$$G_{\mu\nu} = 8\pi T_{\mu\nu} , \tag{7}$$

which couple to f through the definition of the stress-energy tensor,

$$T_{\mu\nu} = \int p_\mu p_\nu \frac{f}{m}\, dV_p . \tag{8}$$

Equations (5)–(8) are the fundamental equations describing relativistic collisionless systems.

For computational convenience, we will consider only systems where all particles have the same rest mass m. (By the equivalence principle, this is not a physically significant restriction for a collisionless system.) In this case equation (5) can be rewritten in the familiar form of equation (1),

$$\frac{\partial f}{\partial t} + \left(\frac{dx^j}{dt}\right)\frac{df}{\partial x^j} + \left(\frac{du_j}{dt}\right)\frac{\partial f}{\partial u_j} = 0 , \tag{9}$$

or, explicitly,

$$\frac{\partial f}{\partial t} + \frac{g^{j\alpha}u_\alpha}{u^0}\frac{\partial f}{\partial x^j} - \frac{1}{2u^0}\, g^{\mu\nu}{}_{,j}\, u_\mu u_\nu \frac{\partial f}{\partial u_j} = 0 , \tag{10}$$

where now $f = f(t, x^j, u_j) \equiv dN/(dV_x\, dV_u)$, with $u_\alpha \equiv p_\alpha/m$, and

$$dV_u \equiv \frac{1}{m^3}\int dV_p\, \delta[(-p_\alpha p^\alpha)^{1/2} - m] = \frac{du_1\, du_2\, du_3}{u^0\sqrt{-g}} \tag{11}$$

is the volume element in velocity space.

b) Choice of Coordinates

From now on we specialize to spherical symmetry. The metric is written in the ADM form (Arnowitt, Deser, and Misner 1962), with isotropic radial coordinate,

$$ds^2 = -(\alpha^2 - A^2\beta^2)dt^2 + 2A^2\beta\, dr\, dt + A^2(dr^2 + r^2\, d\theta^2 + r^2 \sin^2\theta\, d\phi^2) . \tag{12}$$

Here α and β are the lapse and shift functions of ADM; see also Smarr and York (1978*a*, *b*).

As coordinates in phase space, we use the radial velocity u_r, the "angular momentum at infinity" j, defined by

$$j \equiv \sqrt{u_\theta^2 + \frac{u_\phi^2}{\sin^2\theta}} , \tag{13}$$

and the angle

$$\psi \equiv \tan^{-1}\left(\frac{u_\theta \sin\theta}{u_\phi}\right) , \tag{14}$$

measuring the orientation of the transverse velocity. In spherical symmetry, f cannot depend on ψ, and j is a conserved quantity, so that equation (10) reduces to the simple form

$$\frac{\partial f}{\partial t} + \left(\frac{dr}{dt}\right)\frac{\partial f}{\partial r} + \left(\frac{du_r}{dt}\right)\frac{\partial f}{\partial u_r} = 0 , \tag{15}$$

since $\partial f/\partial\psi = 0$ and $dj/dt = 0$. The coefficients dr/dt and du_r/dt can be written explicitly in terms of r, u_r, and the metric coefficients. After some calculation, one finds

$$\frac{dr}{dt} = \frac{u_r}{A^2u^0} - \beta , \tag{16}$$

$$\frac{du^r}{dt} = -u^0\alpha\alpha_{,r} + u_r\beta_{,r} + \frac{u_r^2}{u^0}\frac{A_{,r}}{A^3} + \frac{j^2}{u^0}\left(\frac{1}{r^3A^2} + \frac{A_{,r}}{r^2A^3}\right) , \tag{17}$$

where

$$u^0 = \frac{1}{\alpha}\sqrt{1 + \frac{u_r^2}{A^2} + \frac{j^2}{A^2r^2}} . \tag{18}$$

Equation (17) is simply the geodesic equation corresponding to the metric (12), while equation (18) is obtained from the normalization conditions $u_\alpha u^\alpha = -1$.

The field equations in the metric (12) have been discussed in detail in ST1. We will therefore only mention those key results that are used directly in our numerical scheme. An essential consequence of spherical symmetry is that the metric coefficients can be determined entirely from the ADM *constraint equations*. These are the Hamiltonian constraint equation (ST1, eq. [26]), which here reduces to

$$\frac{1}{r^2}\frac{\partial}{\partial r}\left(r^2\frac{\partial}{\partial r}A^{1/2}\right) = -\frac{1}{4}A^{5/2}\left(8\pi\rho + \frac{3}{4}K^2\right) , \tag{19}$$

and the momentum constraint equation (ST1, eq. [25]), which can be integrated to give

$$K = -\frac{8\pi}{A^3r^3}\int_0^r A^3r^3t_r\, dr . \tag{20}$$

In these expressions, $K = K_r{}^r$ is the radial component of the extrinsic curvature, while ρ and t_r are matter variables as mea-

sured by the normal observers:

$$\rho = T_{\mu\nu} n^\mu n^\nu , \tag{21}$$

$$t_r = \gamma_{r\alpha} n_\beta T^{\alpha\beta} . \tag{22}$$

The vector n^μ is the normal to the t = constant hypersurfaces, described by the three-metric $\gamma^{\mu\nu} \equiv g^{\mu\nu} + n^\mu n^\nu$. The normal has components

$$n_\mu = (-\alpha, 0, 0, 0), \qquad n^\mu = \frac{1}{\alpha}(1, -\beta, 0, 0) . \tag{23}$$

As in ST1, we adopt maximal time slicing, which requires that the trace of the extrinsic curvature tensor vanish. This gives an equation for the lapse function α:

$$\frac{1}{r^2}\frac{\partial}{\partial r}\left(Ar^2 \frac{\partial}{\partial r}\alpha\right) = \alpha A^3\left(8\pi\rho + \frac{3}{2}K^2 + 4\pi T\right), \tag{24}$$

where $T = T^\mu{}_\mu$. Finally, a shift condition is obtained by requiring that the spatial part of the metric be in the isotropic (conformally flat) form of equation (12), which yields

$$\beta = -\frac{3}{2} r \int_r^\infty \frac{\alpha K}{r}\, dr . \tag{25}$$

Once the source terms ρ, K, and T have been determined (see § III*c*), equations (19), (24), and (25) can be solved for the metric coefficients α, A, and β if one imposes appropriate boundary conditions. These are $\alpha_{,r} = A_{,r} = \beta = 0$ at $r = 0$ and $\alpha = A = 1$, $\beta = 0$ at $r = \infty$. However, for numerical work, one must replace the boundary conditions at $r = \infty$ by asymptotic expressions at large but finite r. These conditions can be written (see ST1, but note the wrong sign in their eq. [41]):

$$A = \left(1 + \frac{M}{2r}\right)^2 + O\left(\frac{M^4}{r^4}\right), \tag{26}$$

$$\alpha = \frac{\left(1 - \frac{M}{2r}\right)}{\left(1 + \frac{M}{2r}\right)} + O\left(\frac{M}{r}\right), \tag{27}$$

$$\beta = -\frac{1}{2} rK + O\left(\frac{M^3}{r^3}\right), \tag{28}$$

where the lowest order terms are used as boundary conditions at $r \gg M$. Here M is the total mass-energy of the system, which can be calculated from the values of the metric coefficients outside the surface of the matter as (see ST1, § III*e* for a derivation)

$$M = \frac{1}{2} Ar\left[1 + \frac{1}{4}(ArK)^2 - \left(1 + \frac{r}{A} A_{,r}\right)^2\right]. \tag{29}$$

This is not to be confused with the total *rest mass* of the system, M_0, which by definition of f can be written

$$M_0 = m \int f dV_x dV_u . \tag{30}$$

A very useful quantity derived from M and M_0 is the binding energy per particle in the system, or *fractional binding energy*, $E_b/M_0 \equiv 1 - M/M_0$.

c) Source Terms

The source terms ρ, K, and T appearing in the field equations (19), (24), and (25) are now computed explicitly in terms of the distribution function f. Combining equations (8) and (21), we get, after some calculation,

$$\rho = m \int (\alpha u^0)^2 f dV_u . \tag{31}$$

Similarly, equations (8) and (22) give

$$t_r = -m \int (\alpha u^0)(fu_r) dV_u , \tag{32}$$

$$T = -m \int f dV_u . \tag{33}$$

This agrees with equations (43), (45), and (46) of ST1, if one replaces their discrete sum over particles by a quadrature over velocity space. The volume element in velocity space dV_u, defined by equation (11), must now be written in terms of our phase space coordinates u_r, j, and ψ. Since for the metric (12), $(-g)^{1/2} = A^3 \alpha r^2 \sin\theta$, we get from the equations (11)–(14),

$$dV_u = \frac{du_r\, du_\theta\, du_\phi}{A^3 r^2 \alpha u^0 \sin\theta} = \frac{\pi}{A^3 r^2 \alpha u^0}\, dj^2\, du_r , \tag{34}$$

where the integral over ψ has been carried out in the last expression. Finally, if we combine equations (31)–(34) and (20), the calculation of the source terms is reduced to the three following quadratures:

$$K = \frac{8\pi^2 m}{A^3 r^3} \int_0^r dr \int_0^{+\infty} dj^2 \int_{-\infty}^{+\infty} du_r (fru_r) , \tag{35}$$

$$\rho = \frac{\pi m}{A^3 r^2} \int_0^{+\infty} dj^2 \int_{-\infty}^{+\infty} du_r f\left(1 + \frac{u_r^2}{A^2} + \frac{j^2}{A^2 r^2}\right)^{1/2} , \tag{36}$$

$$T = -\frac{\pi m}{A^3 r^2} \int_{-\infty}^{+\infty} dj^2 \int_{-\infty}^{+\infty} du_r f\left(1 + \frac{u_r^2}{A^2} + \frac{j^2}{A^2 r^2}\right)^{-1/2} . \tag{37}$$

Care must be taken of how these expressions are evaluated at $r = 0$, where $f \neq 0$ only for $j = 0$. The coordinate singularity at $r = 0$ in equations (35)–(37) is eliminated by rewriting the volume element in velocity space $dV_u = dv_{\hat{x}}\, dv_{\hat{y}}\, dv_{\hat{z}}$ instead of equation (34), where carets indicate components in an orthonormal frame of reference. Since $r = 0$ is a center of symmetry, f there can depend only on the magnitude $v \equiv (v_{\hat{x}}^2 + v_{\hat{y}}^2 + v_{\hat{z}}^2)^{1/2}$ of the velocity vector. Therefore we can also write $dV_u = 4\pi v^2\, dv$, so that we finally get

$$K_c = 0 , \tag{38}$$

$$\rho_c = 4\pi m \int_0^{+\infty} dv f_c(v) v^2 (1 + v^2)^{1/2} , \tag{39}$$

$$T_c = -4\pi m \int_0^{+\infty} dv f_c(v) v^2 (1 + v^2)^{-1/2} , \tag{40}$$

Here a subscript c indicates a value at $r = 0$ and $f_c(v) \equiv f(r = 0, j = 0, u_r = A_c v)$.

d) Newtonian Limit

In the Newtonian limit, $A \to 1$, $u^0 \to 1$, $\beta \to 0$, $\alpha \to 1$, and $\alpha_{,r} \to \Phi_{,r}$, where Φ is the Newtonian potential. Therefore, equations (15)–(18) simply reduce to (Fujiwara 1983).

$$\frac{\partial f}{\partial t} + v_r \frac{\partial f}{\partial r} + \left(\frac{j^2}{r^3} - \Phi_{,r}\right)\frac{\partial f}{\partial v_r} = 0 , \tag{41}$$

where now $v_r \equiv dr/dt$ and $j \equiv rv_\perp$ are the usual radial velocity

and angular momentum in spherical coordinates. The force per unit mass $-\Phi_{,r}$ can be directly calculated as

$$-\Phi_{,r} = -\frac{M(r)}{r^2} = -\frac{4\pi^2 m}{r^2}\int_0^r dr \int_0^\infty dj^2 \int_{-\infty}^\infty dv_r\, f\,. \quad (42)$$

This is easily obtained by directly integrating equation (24) in the Newtonian limit.

Finally, the Newtonian kinetic energy T and potential binding energy W are computed as

$$T = 2\pi^2 m \int_0^\infty dr \int_0^\infty dj^2 \int_{-\infty}^\infty dv_r \left(v_r^2 + \frac{j^2}{r^2}\right) f\,, \quad (43)$$

and

$$W = 4\pi \int_0^\infty M(r)\rho r\, dr\,, \quad (44)$$

so that the total (conserved) energy $E = T - W$.

IV. THE NUMERICAL SCHEME

We now discuss several new features of our numerical method, especially those concerning the construction of the distribution function and the calculation of the matter source terms for the field equations. The reader is referred to ST1, § IV for a description of how the field equations (19) and (24) can be solved numerically.

Of all the refinements introduced in our code to make it more efficient, the use of a *self-adaptive quadrature routine* (see, e.g., Forsythe *et al.* 1977) proved to be most essential. Instead of computing the values of f on a fixed grid of points in velocity space and then summing these values by the trapezoidal rule, a self-adaptive routine asks for values of f only at those points where they are really needed to maintain a specified accuracy. This clearly minimizes the number of points where the distribution function has to be evaluated. Moreover, any discontinuity in the initial data will be automatically and accurately treated. The self-adaptive routine will simply add a sufficiently large number of points on either side of the discontinuity to locate its position accurately enough before integrating across.

In our code we use the NAG (1980) routine D01AJF for all one-dimensional quadratures (eqs. [39]–[40]) and D01FCF for all multidimensional quadratures (eqs. [35]–[37]). Both routines call a user-defined function which returns the value of the integrand at a given point. In this function, f is evaluated numerically by integrating a trajectory backward in time, from a point (r, u_r, j) in phase space to $t = 0$, in the known metric, as discussed in § II. This trajectory is constructed by solving the two ordinary differential equations (16) and (17) via a numerical scheme based on the Bulirch-Stoer algorithm (see, e.g., Press *et al.* 1986) which allows rather large step sizes to be taken. Near turning points, however, the step size must be reduced, and the scheme switches to a fourth-order Runge-Kutta method for better efficiency.

The right-hand sides of equations (16) and (17) involve values of the fields and their derivatives, which therefore must be stored, for all iterations, on a radial grid. Methods for constructing such a radial grid and adapting its structure to the evolving matter were discussed in ST1, § IV. Since this radial grid is also used to solve the field equations by finite differences, the number of grid points must be rather large (typically we used 512). However, by construction, the matter variables change very little from one grid point to the next, so that it is, of course, not necessary to repeat the quadratures over velocity space at every radial grid point. In practice, quadratures are only computed at a relatively small number of *representative radial points* (typically 16), and interpolation between representative points is used to determine the values of the source terms at all other radial grid points. The interpolation scheme we use is based on an algorithm by Fritsch and Carlson (1980). In contrast to cubic splines, this very robust scheme automatically conserves the monotonicity properties of the data to be interpolated. A first representative point is always placed at $r = 0$, where quadratures reduce to one dimension, equations (39)–(40), and are therefore especially easy to evaluate. Other representative points must cover the matter up to its outer surface. The actual number of representative points needed depends on the degree of central condensation in the system and on the desired accuracy (typically 1% in our calculations). In Figure 1 we have sketched the logical flow in our code, which consists of ~2500 FORTRAN lines broken up into 60 small subroutines.

Typically, relativistic initial conditions are given in the form

$$f = \begin{cases} F(x), & \text{for } x \equiv p_{\hat{0}}/E_{\max} \le 1\,, \\ 0, & \text{for } x > 1\,, \end{cases} \quad (45)$$

where $p_{\hat{0}}$ is the energy of a particle measured by a normal observer, and $E_{\max}$ is the value of $p_{\hat{0}}$ at the surface of the matter. The initial matter and metric profiles are obtained by integrating numerically the familiar equations of structure for spherical equilibrium clusters (see, e.g., Ipser and Thorne 1968; ST1).

Each main iteration consists in choosing a new time step, radial mesh, and set of representative points, then computing the source terms, and finally solving the field equations. As in ST4, we choose the time step $\Delta t = q t_{\rm dyn}$, where q is $\lesssim 1$ (typically $q = 0.1$) and $t_{\rm dyn}$ is the *central* (minimum) free-fall *proper* time scale:

$$t_{\rm dyn} = \frac{1}{\alpha_c}\sqrt{\frac{3\pi}{32\rho_c}}\,. \quad (46)$$

The output of our code consists of the values of the metric coefficient A, α, and β, and the matter variables ρ, T, and K for all radial grid points and all iterations. Postanalysis of this output is done with a separate code which produces spacetime diagrams containing Lagrangian matter tracers, light ray tracers, and possible horizons, contour plots of the distribution function in two-dimensional slices of phase space, and various radial profiles of fields and matter variables (the equations relevant to this postanalysis are given in ST1 § III*e*). The only diagnostic performed within the main code is the calculation of the total mass-energy of the system (eq. [29]) which should be conserved in time.

For all Newtonian calculations, we used a slightly modified version of the code where equation (41) is used explicitly. In particular, the *three-dimensional* quadrature of equation (42) is performed numerically (using the same NAG routine as above). This procedure gives the values of the force per unit mass at representative points (typically 30) directly, eliminating the evaluation of $\phi_{,r}$ by finite differencing.

V. APPLICATIONS

a) Newtonian Clusters

As a first test-bed calculation, we checked how accurately our Newtonian code could maintain the structure of a *stable*

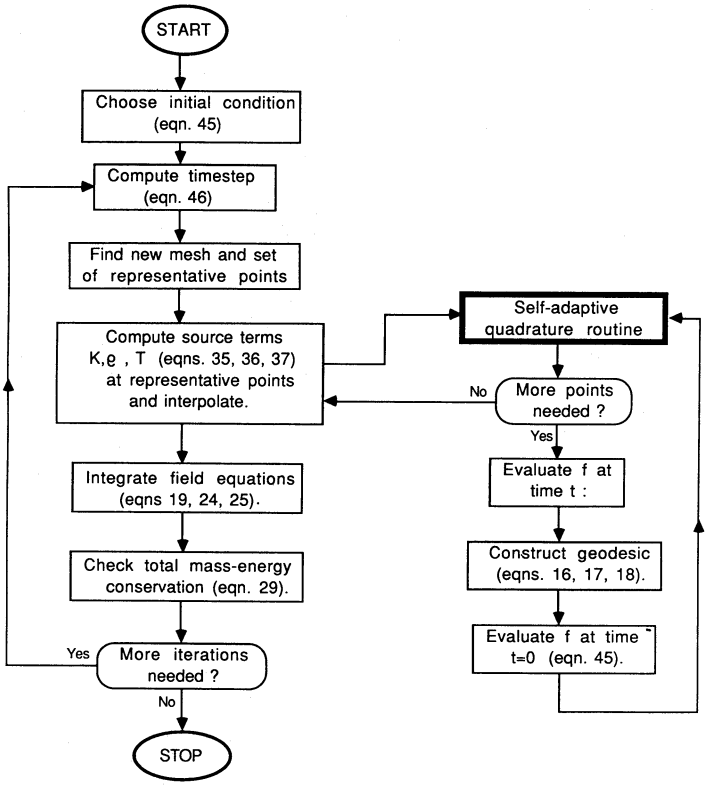

FIG. 1.—Logical flow chart of relativistic code. Note the central role of the self-adaptive quadrature routine. See text for details.

equilibrium cluster. The initial condition was chosen to have the form of an $n = 5$ polytrope (a Plummer law) which is known to be stable (Antonov 1962):

$$f(E) = \begin{cases} K|E|^{7/2}, & \text{for } E \le 0\,, \\ 0, & \text{for } E > 0\,, \end{cases} \tag{47}$$

where

$$E = -\frac{GM}{a}\left(1 + \frac{r^2}{a^2}\right)^{-1/2} + \frac{1}{2}\left(u_r^2 + \frac{j^2}{r^2}\right) \tag{48}$$

is the energy of a star per unit mass. This is a convenient choice because equations (47) and (48) give f explicitly as a function of coordinates in phase space, without having to integrate structure equations for spherical equilibrium (here the Lane-Emden equation).

We compared the mass profile at $t = 0$ as computed from equations (47)–(48),

$$M_r = M\left(\frac{r^3}{a^3}\right)\left(1 + \frac{r^2}{a^2}\right)^{-3/2}, \tag{49}$$

with the mass profile output by our code after the system has been evolved for 15 dynamical times, where here the dynamical time $t_{\rm dyn} \equiv (a^3/GM)^{1/2}$. We found that the structure was very accurately maintained, the maximum difference between the two profiles being $\Delta M_r/M = 0.015$ at $r/a = 1.8$. Conservation of total mass and energy during this run were achieved to better than 0.5%. Here all integration parameters had the "typical" values mentioned in § IV, and the total computation time was ~ 1.5 hr on an IBM 3090-600.

Next we turn to a nonequilibrium initial condition, i.e. one with a virial ratio $2T/W < 1$ at $t = 0$. We construct it by reducing all velocities by a constant factor in the Plummer model considered above. This is done by making the substitutions $u \mapsto \alpha u$ and $j \mapsto \alpha j$ in equation (48), where $\alpha > 1$. This *reduces* the kinetic energy T of the system by a factor $1/\alpha^2$ but leaves the mass profile M_r and potential energy W unchanged. Here we chose $\alpha = 2^{1/2}$ so that $2T/W = 0.5$ initially.

The time evolution of the virial ratio is presented in Figure 2. As expected, the cluster collapses in a few dynamical times and evolves, via phase mixing and violent relaxation, to a new equilibrium state ($2T/W \to 1.0$). In this case the collisionless damping due to phase mixing is rapid, and virial equilibrium is reached after essentially just one collective oscillation. We also compare in Figure 2 the results of this run to those obtained by an entirely different method: a *concentric shell* method (see Henon 1964), first with 5000 shells (*dotted line*), then with 20,000 shells (*dashed line*). In both cases the agreement between the two methods is very good, but it is striking to see that the agreement is much better with 20,000 shells than with 5000 shells, suggesting that, as expected from a phase space method, the solution constructed by our code does indeed correspond to the $N \to \infty$ limit. Figure 3 illustrates how large degrees of phase mixing can be accurately treated by our method. Here the time evolution of the distribution function is shown, inside a plane of constant angular momentum. Finally, Figure 4 shows the relaxed mass profile obtained by our code, and a comparison with those obtained by the concentric shell method. Again the agreement is excellent, especially when a large number of shells is used.

For completeness, we also examined the collapse of a homogeneous sphere with Maxwellian *kinetic* energy distribution:

$$f = \begin{cases} \left(\frac{3M}{4\pi R^3}\right)\left(\frac{1}{2\pi\sigma^2}\right)^{3/2} \exp\left(-\frac{u^2 + j^2/r^2}{2\sigma^2}\right), & \text{if } r \le R\,; \\ 0, & \text{if } r > R\,. \end{cases} \tag{50}$$

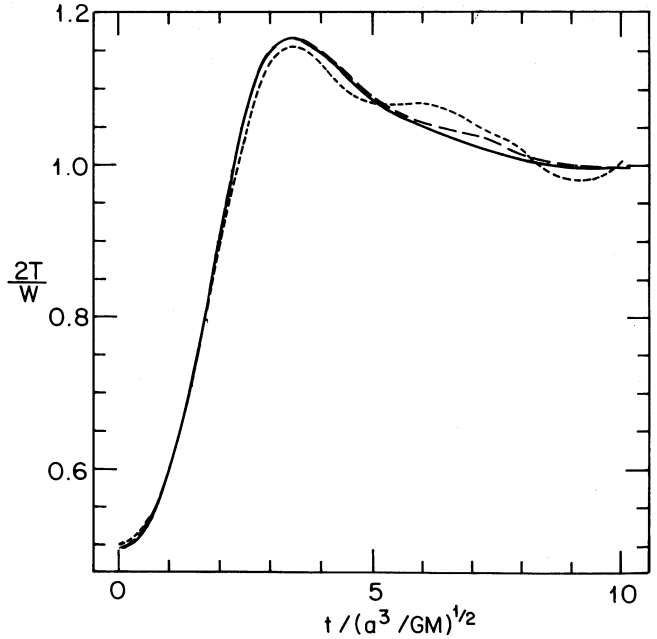

FIG. 2.—Evolution of the virial ratio $2T/W$ for a destabilized Plummer model. Short-dashed line is from a concentric shell model with 4000 shells. Long-dashed line is from the same concentric shell model, but with 20,000 shells. Solid line is from solving the collisionless Bolzmann equation by our method. As expected, the agreement gets better when the number of shells is increased.

Such an initial condition was also considered in previous studies of Newtonian collisionless systems by Hénon (1964), Hoffman *et al.* (1979), and Fujiwara (1983). However, it has the rather unnatural features that a fraction of the matter is unbounded initially and escapes from the system (no energy cutoff), and that f has a sharp discontinuity, which is located at $r = 0$ initially, but then propagates in phase space and is present at all times. In Figures 5 and 6, we have compared our results with those obtained by a *direct N-body simulation*, first with 1000, then with 2000 particles. Again the agreement is good, but becomes better when a larger number of particles is used.

b) Relativistic Star Clusters

Following historical tradition (Zel'dovich and Podurets 1965; Fackerell 1966; Ipser 1969; ST2), we first consider the dynamical evolution of a collisionless system initially in equilibrium and characterized by a *truncated isothermal* distribution function, i.e., with $F(x) = K \exp(-x/T')$ in equation (45), where K is a normalization constant and $T' = T/E_{\max}$ is the reduced temperature. As in the previous investigations, we examine the one-parameter sequence of models obtained by imposing the constraint $E_{\max} = m - 0.5T$, where m is the rest mass of a star.

Figure 7 shows the time evolution of the central redshift for several models along the sequence. The transition between stability and instability is clearly located at central redshift $Z_c = 0.42$, in complete agreement with the results of ST2. Figures 8 and 9 show the spacetime evolution of the unstable model with $Z_c = 0.517$. In a few dynamic times, the system collapses to a black hole, which is identified by the presence of an event horizon and a region of trapped surfaces. The properties of the limit surface are in excellent agreement with ST4. For example, the inner boundary of the region of trapped surfaces exactly coincides with the Lagrangian matter tracer corresponding to an interior rest-mass fraction of 0.5 (see ST4, Fig. 11).

The unique character of our method is revealed in Figure 10, which shows how this collapse proceeds in *phasespace*. The coordinates used here are not the same as in § III. Instead, we use the Schwarzschild areal radius r_S and the radial velocity $u^{\hat{r}} = u_r/(A\alpha u^0)$ measured by a *normal* observer. As shown in ST4, r_S and $u^{\hat{r}}$ are *freezing variables*, i.e., they become constant (with t) at late times wherever the lapse of proper time in the normal observer's reference frame goes to zero. Therefore we

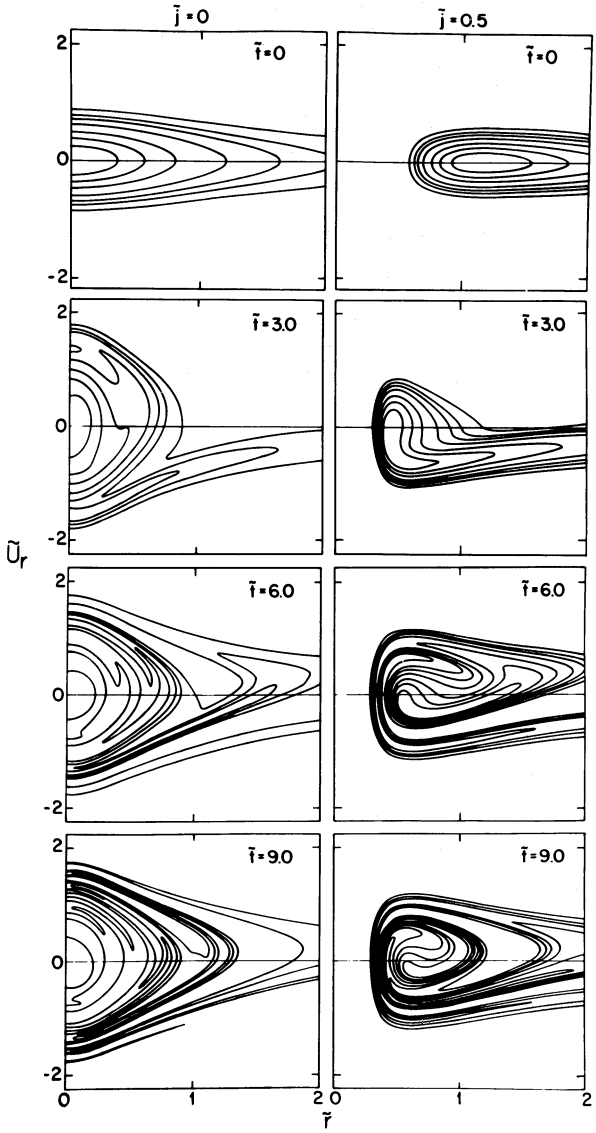

FIG. 3.—Evolution of the distribution function for the destabilized Plummer model considered in Fig. 2. This illustrates how our code can handle distribution functions with complicated structures (in this case due to phase mixing and violent relaxation). The nondimensional quantities used here are defined as follows: $\tilde{r} = r/a$, $\tilde{u}_r = u_r/(GM/a)^{1/2}$, $\tilde{j} = j/(GMa)^{1/2}$, $\tilde{t} = t/(a^3/GM)^{1/2}$. Each plane $(\tilde{r}, \tilde{u}_r)$ is a two-dimensional slice taken from the three-dimensional phase space by setting the angular momentum per unit mass j equal to a constant. The sequence on the left shows the evolution in the $j = 0$ plane, whereas that on the right corresponds to $j = 0.5(GM)^{1/2}$, a "typical" nonzero value. Lines of constant f are shown, equally spaced between 0 and its maximum value in the slice. (Note that for $j \neq 0$, the matter can never reach $r = 0$.)

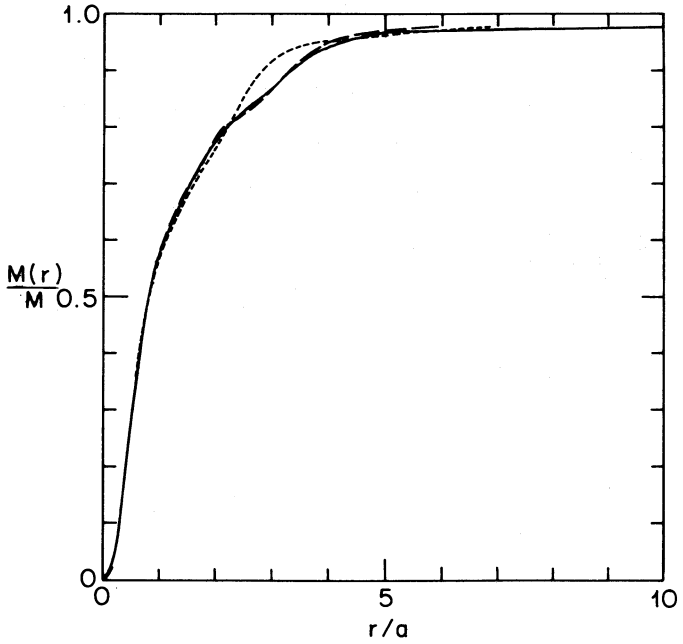

FIG. 4

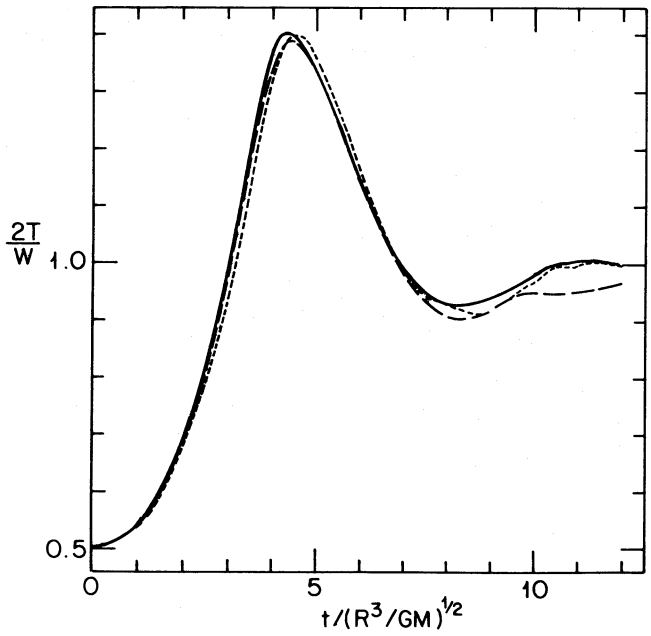

FIG. 5

FIG. 4.—Final (relaxed) mass profile for the destabilized Plummer model considered in Fig. 2. Notations are as in Fig. 2.

FIG. 5.—Evolution of the virial ratio $2T/W$ for a cluster initially homogeneous and isothermal (eq. [50]). Short-dashed line is from a direct N-body simulation with 1000 particles. Long-dashed line is from a similar N-body simulation with 2000 particles. Solid line is from our method.

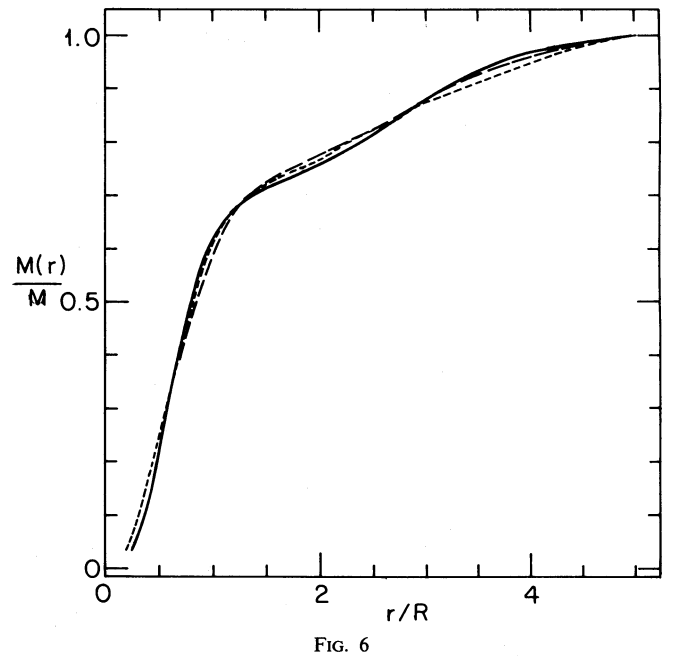

FIG. 6

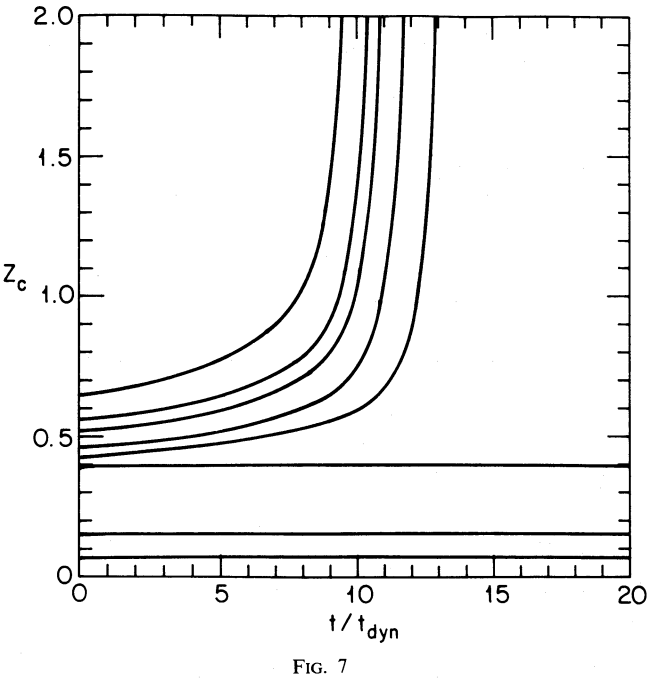

FIG. 7

FIG. 6.—Final (relaxed) mass profile for the case considered in Fig. 5. Notations are as in Fig. 5.

FIG. 7.—Time evolution of the central redshift Z_c for several clusters initially taken along the truncated isothermal sequence. Here the unit of time t_{dyn} (see eq. [46]) is the central (minimum) free-fall proper time scale. (Note that its numerical value is different for each cluster along the sequence.) The three models at the bottom are stable: our calculations reveal no change of structure on a dynamical time scale. The five models having initial redshifts larger than $Z_c = 0.42$ are unstable: they collapse to black holes in a few dynamical times.

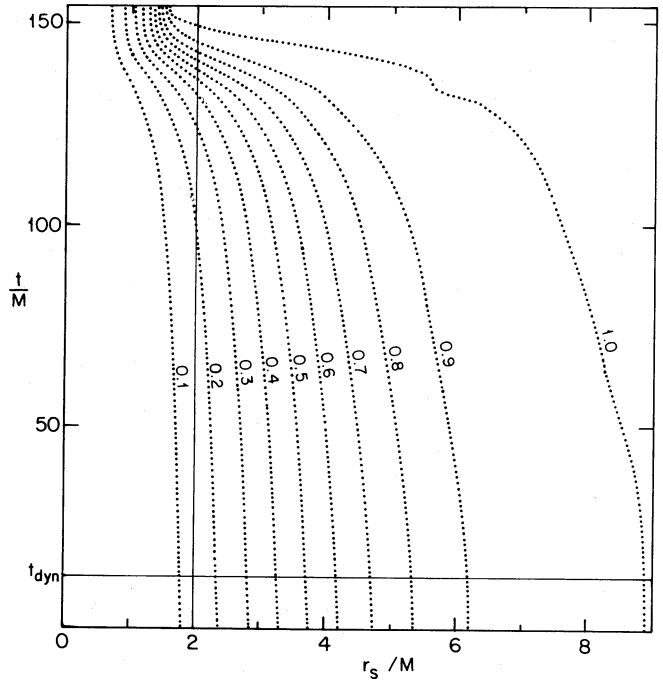

FIG. 8.—Spacetime diagram showing the evolution of an unstable cluster undergoing catastrophic collapse to a black hole. Both the Schwarzschild radius r_S and the time t are measured in units of the total mass-energy M of the cluster. Initially, the cluster is in equilibrium and has a truncated isothermal distribution with central redshift $Z_c = 0.52$. Dotted lines are the world lines of fictitious Lagrangian matter tracers labeled by their fixed interior rest-mass fractions.

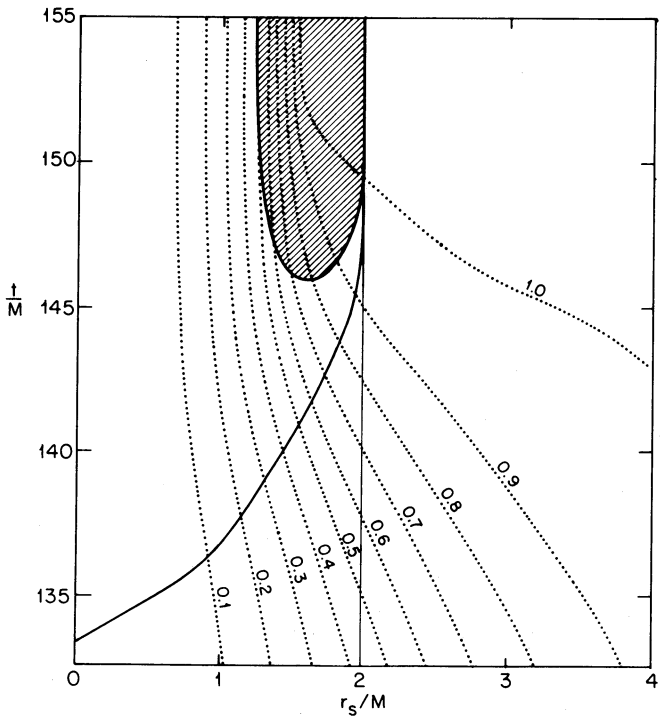

FIG. 9.—Detail of the spacetime structure near the formation of an event horizon for the unstable case shown in Fig. 8. Dotted lines are the world lines of fictitious Lagrangian matter tracers labeled by their fixed interior rest-mass fractions. Solid line is the event horizon. Shaded area is the region of trapped surfaces.

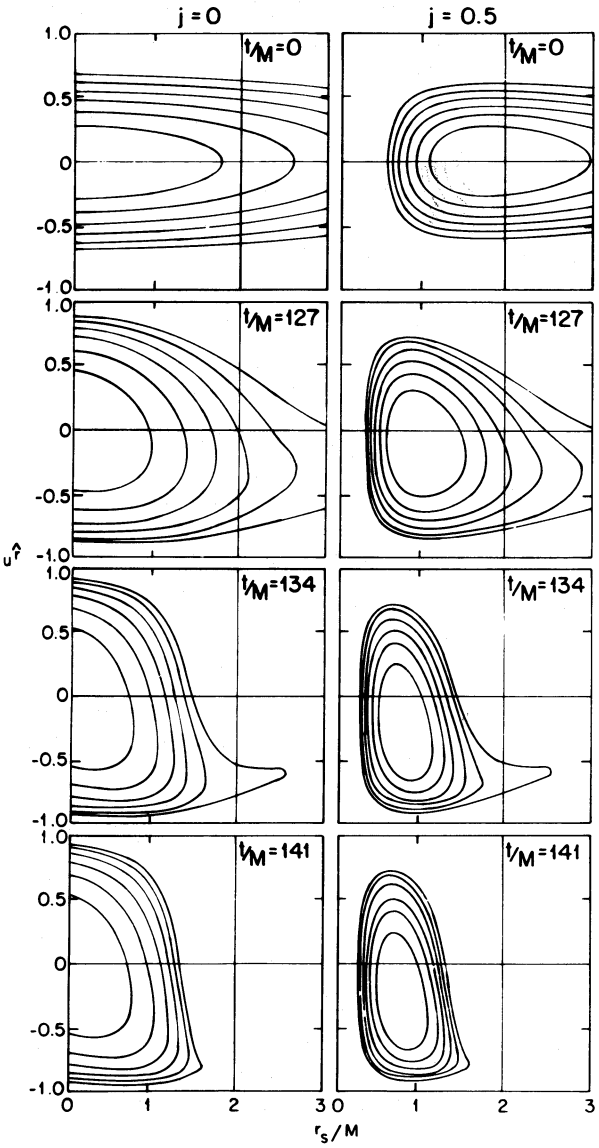

FIG. 10.—Time evolution of the distribution function for a cluster undergoing catastrophic collapse to a black hole. Initially, the cluster has a truncated isothermal distribution with central redshift $Z_c = 0.52$. The Schwarzschild radius r_S (in units of the total mass-energy M) and the radial velocity $u^{\hat{r}}$ are used as phase space coordinates. Each plane (r_S, $u^{\hat{r}}$) is a two-dimensional slice taken from the three-dimensional phase space by setting the angular momentum j (see eq. [13]) equal to a constant. The series on the left corresponds to $j = 0$, whereas that on the right corresponds to $j = 0.5M^2$, which represents the angular momentum of a "typical star" in this cluster ($0 \leq j \lesssim M^2$ for $f \neq 0$). Lines of constant f are shown, equally spaced between 0 and its maximum value in the slice. (Note that for $j \neq 0$, the matter never reaches $r_S = 0$.) In the final plots, the entire mass of the cluster has collapsed inside an event horizon located at $r_S = 2M$.

expect the distribution function expressed in these variables to exhibit a steady configuration at late coordinate time, wherever $\alpha \to 0$. This is indeed what we find: once all the matter with a given value of j has collapsed inside the horizon, the distribution function very slowly evolves toward a final steady structure, symmetric with respect to $\pm u^{\hat{r}}$. It is striking to see how different this relativistic collapse is from the typical Newtonian collapse depicted in Figure 3. There is essentially no phase mixing here, and the distribution function evolves very "quietly" toward its final state.

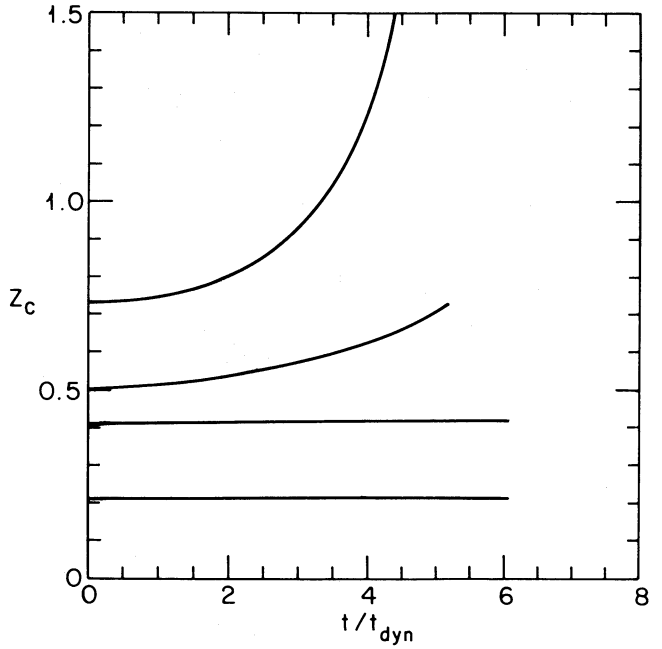

FIG. 11.—Time evolution of the central redshift Z_c for several clusters initially taken along the $n = 4$ polytropic sequence. As before, the unit of time, t_{dyn} (see eq. [46]), is the central free-fall proper time of each cluster. All models having at $t = 0$ a central redshift larger $Z_c = 0.42$ are found to be unstable. The onset of instability therefore appears to coincide with the first maximum of the fractional binding energy along the sequence.

We also looked at the stability of the $n = 4$, relativistic, polytropic equilibrium sequence originally examined by Fackerell (1970). In this case $F(x) = Kx^{-5}(1 - x^2)^{5/2}$ in equation (45). These clusters are important because, unlike the truncated isothermal models, they are characterized by extreme core-halo structures. Apart from their unique computational aspects, these structures may be of significant astrophysical relevance. Indeed, as discussed in ST3, if relativistic star clusters ever form in nature, they are likely to be very centrally condensed. In Figure 11 we show the time evolution of the central redshift for several models along the sequence. The models having an initial central redshift $Z_c \geq 0.42$ are found to be unstable and collapse to black holes. This is just past the first maximum of the fractional binding energy (E_b/M) along the sequence (see, e.g., Fackerell 1970). Our results completely confirm those obtained in previous investigations, thereby providing again compelling numerical evidence that Ipser's (1980) conjecture, that, as in the case of fluid stars, the instability sets in precisely *at the first fractional binding energy maximum* along the sequence, is in fact true.

In all the equilibrium sequences that we studied, the clusters become unstable when their central redshift $Z_c \gtrsim 0.5$. This had already been found in the semianalytical calculations of Ipser (1969*a*, *b*) and Fackerell (1970). It had generally been believed since then that all relativistic star clusters with central redshift $Z_c \gtrsim 0.5$ should be dynamically unstable. One may wonder, however, whether it is possible to construct an equilibrium sequence of relativistic clusters where the fractional binding energy monotonically increases with redshift. Would all clusters, in such a sequence, remain stable even when $Z_c \gg 0.5$? We have addressed these important questions using our new code and found that it is indeed possible to construct stable relativistic star clusters with arbitrarily large central redshifts. A detailed description of the construction procedure, together with a complete stability analysis, have been published elsewhere (see Rasio *et al.* 1989).

It is a great pleasure to thank D. Chernoff and M. Weinberg for stimulating discussions and for providing us with their own results of some of the Newtonian cases considered in § V. We also thank G. Quinlan for helping us in developing the interpolation scheme mentioned in § IV. This work has been supported by National Science Foundation grants AST 87-14475 and PHY 86-03284 to Cornell University. Computations were performed on the Cornell National Supercomputer Facility, which receives support from the National Science Foundation, IBM corporation, New York State, and members of the Cornell Research Institute.

REFERENCES

Antonov, V. A. 1962, *Vest. Leningrad Gos. Univ.*, **19**, 96.
Arnowitt, R., Deser, S., and Misner, C. W. 1962, in *Gravitation*, ed. L. Witten (New York: Wiley), p. 227.
Begelman, M. C., Blandford, R. C., and Rees, M. J. 1984, *Rev. Mod. Phys.*, **56**, 255.
Bisnovatyi-Kogan, G. S., and Thorne, K. S. 1970, *Ap. J.*, **160**, 875.
Centrella, J. M., LeBlanc, J. M., and Bowers, R. L., eds. 1985, *Numerical Astrophysics* (Boston: Jones & Bartlett).
Choptuik, M. W. 1986, Ph.D. thesis, University of British Columbia.
Cuperman, S., and Harten, A. 1972*a*, *Astr. Ap.*, **16**, 13.
———. 1972*b*, *Ap. Space Sci.*, **18**, 207.
Cuperman, S., Harten, A., and Lecar, M. 1971, *Ap. Space Sci.*, **13**, 411.
Dawson, J. M. 1983, *Rev. Mod. Phys.*, **55**, 403.
Dressler, A., and Richstone, D. O. 1988, *Ap. J.*, **324**, 701.
Fackerel, E. D. 1968, *Ap. J.*, **153**, 643.
———. 1970, *Ap. J.*, **160**, 859.
Forsythe, G. E., Malcolm, M. A., and Moler, C. B. 1977, *Computer Methods for Mathematical Computations* (Englewood Cliffs: Prentice-Hall).
Fritsch, F. N., and Carlson, R. E. 1980, *Siam J. Numer. Anal.*, **17**, 238.
Fujiwara, T. 1981, *Pub. Astr. Soc. Japan*, **33**, 531.
———. 1983, *Pub. Astr. Soc. Japan*, **35**, 547.
Heńon, M. 1964, *Ann. d' Ap.*, **27**, 83.
Hoffman, Y., Shlosman, I., and Shaviv, G. 1979, *M.N.R.A.S.*, **189**, 737.
Hohl, F. H., and Feix, M. R. 1967, *Ap. J.*, **147**, 1164.
Inagaki, S., Nishida, M. T., and Sellwood, J. A. 1984, *M.N.R.A.S.*, **210**, 589.
Ipser, J. R. 1969*a*, *Ap. J.*, **156**, 509.
Ipser, J. R. 1969*b*, *Ap. J.*, **158**, 17.
———. 1980, *Ap. J.*, **238**, 1101.
Ipser, J. R., and Thorne, K. S. 1968, *Ap. J.*, **154**, 251.
Kochanek, C. S., Shapiro, S. L., and Teukolsky, S. A. 1987, *Ap. J.*, **320**, 73.
Kormendy, J. 1988, *Ap. J.*, **325**, 128.
Lightman, A. P., and Shapiro, S. L. 1978, *Rev. Mod. Phys.*, **50**, 437.
Luwel, M., and Severne, G. 1985, *Astr. Ap.*, **152**, 305.
Lynden-Bell, D. 1967, *M.N.R.A.S.*, **136**, 101.
Misner, C. W., Thorne, K. S., and Wheeler, J. A. 1973, *Gravitation* (San Francisco: Freeman).
NAG. 1980, *Fortran Library Manual Mark 8* (NAG Central Office, 7 Banbury Road, Oxford OX2 6NN, UK) Chapter D01.
Nishida, M. T. 1986, *Ap. J.*, **302**, 611.
Press, W. H., Flannery, B. P., Teukolsky, S. A., and Vetterling, W. T. 1986, *Numerical Recipe* (Cambridge: Cambridge University Press).
Quinlan, G. D., and Shapiro, S. L. 1987, *Ap. J.*, **321**, 199.
Rasio, F. A., Shapiro, S. L., and Teukolsky, S. A. 1989, *Ap. J.* (*Letters*), **336**, L63.
Sellwood, J. A. 1986, in *Use of Supercomputers in Stellar Dynamics*, ed. S. McMillan and P. Hut (Berlin: Springer), p. 5.
———. 1987, *Ann. Rev. Astr. Ap.*, **25**, 151.
Shapiro, S. L., and Teukolsky, S. A. 1985*a*, *Ap. J.*, **298**, 34 (ST1).
———. 1985*b*, *Ap. J.*, **298**, 58 (ST2).
———. 1985*c*, *Ap. J.* (*Letters*), **292**, 141 (ST3).
———. 1986, *Ap. J.*, **307**, 575 (ST4).
Shlossman, I., Hoffman, Y., and Shaviv, G. 1979, *M.N.R.A.S.*, **189**, 723.

Smarr, L., ed. 1979, *Sources of Gravitational Radiation* (Cambridge: Cambridge Unversity Press).
Smarr, L., and York, J. W. 1978*a*, *Phys. Rev. D*, **17**, 1945.
———. 1978*b*, *Phys. Rev. D*, **17**, 2529.
van Albada, G. B. 1960, *Bull. Astr. Inst. Netherlands*, **15**, 165.
White, R. L. 1983, preprint.
White, R. L. 1986, in *Use of Supercomputers in Stellar Dynamics*, ed. S. McMillan and P. Hut (Berlin: Springer), p. 167.
———. 1988, *Ap. J.*, **330**, 26.
Zel'dovich, Ya. B., and Podurets, M. A. 1965, *Astr. Zh.*, **42**, 963 (English trans. in *Soviet Astr.—AJ*, **9**, 742 [1966]).

FREDERIC A. RASIO, STUART L. SHAPIRO, and SAUL A. TEUKOLSKY: Cornell University, Space Sciences Building, Ithaca, NY 14853